SIMULATION OF CEREBRAL INFUSION TESTS USING A POROELASTIC MODEL

IAN SOBEY, ALMUT EISENTRÄGER, BENEDIKT WIRTH, AND MAREK CZOSNYKA

Abstract. In an infusion test the apparent rate of cerebrospinal fluid (CSF) production is temporarily increased through injection of fluid directly into the CSF system with the result that CSF pressure rises, in theory to a new plateau average, and the change in pressure level gives a measure of resistance to CSF outflow and the rate of approach to the plateau gives information about cerebral compliance. In the first part of this paper we give details of a two-fluid (blood and CSF) spherically symmetric poroelastic model that can simulate an infusion test which includes oscillations in blood pressure. This model has been applied to clinical data where the infusion rate and arterial blood pressure are input and an oscillatory CSF pressure is computed along with spatial parenchyma displacement, strain and local changes in CSF content. In the later part of this paper, the poroelastic model is simplified by spatial integration resulting in a one-compartment model that includes blood pressure oscillations but which, when they are ignored, reduces to a well known one-compartment model. When the arterial pressure pulsations are included, their interaction with a non-linear compliance results in solutions that have to be interpreted very carefully to predict parameter values.

Key words. infusion test, intracranial cerebrospinal fluid pressure, poroelasticity

1. Introduction

The infusion test can be used to aid interpretation of CSF function: for a short period of time the rate of CSF production is increased and the change in CSF pressure is measured. Usually the time average value rises to a new plateau value, the rate of rise giving information about the cerebral compliance and the plateau value showing the resistance to CSF absorption, two important clincial indicators of CSF function. The simplest interpretation of this test assumes that the CSF is contained in a single compliant compartment so that the pressure variation is described by a first order ODE in time with CSF production as input parameter. Such models do not take arterial pressure fluctutation into account and the CSF pressure calculated, while slowly varying in time, does not fluctuate on the scale of arterial pressure pulsations, see for example [8] for a review of such models.

In a series of papers ([9], [10], [13]) a poroelastic model was developed for predicting changes in cerbrospinal fluid pressure in a number of situations, originally for obstructive hydrocephalus and then extended to some time dependent situations. The original model was based on a long time scale so fluctuations in arterial pressure were neglected, indeed that model considered the brain only as a two-phase material with a porous elastic phase through which CSF could move and where changes in CSF pressure (intracranial pressure, ICP) were coupled to changes in stress and strain in the elastic phase. In a more recent paper, [15], a mathematical model was developed that included multiple fluid phases, in individual compartments, separated from each other and where CSF was one of the fluids. Here we develop that model for two fluid compartments, retaining a continuum hypothesis and treating the brain as having three compartments or phases: a porous elastic

compartment, a CSF compartment and a single blood compartment. There is no exchange of fluid between the CSF and blood compartments. Both the elastic and CSF compartments have spatial, as well as temporal, dependence. The model retains spherical symmetry and so is the simplest spatially varying complete model for ICP fluctuations, complete in the sense that the model can be used to simulate changes in ICP in for example, an infusion test. However the spatial dependence means that the model is time consuming to solve numerically. In this paper we set out the spatially varying model and then derive from that model, a spatially averaged model that while still requiring numerical solution, can be integrated rapidly.

2. Spatially varying model

2.1. Biot's theory of poroelastic deformation. In order to derive a three-phase poroelastic model for the brain we begin by briefly reviewing the theory of [2], particularly using the notation described in [11] (see pp17-21 therein). For a fluid-filled, porous, solid matrix, Biot supposed a continuum description with a strain ε, overall stress σ, fluid pressure p, and an additional variable ζ, the increment in fluid content per volume element. Assuming a physical state to be locally described by pressure and stress and linearising the relations between $\varepsilon, \sigma, p, \zeta$ gives that

$$(2.1) \qquad \varepsilon = a_{11}\sigma + a_{12}p,$$

$$(2.2) \qquad \zeta = a_{21}\sigma + a_{22}p.$$

Furthermore, Biot assumed the existence of an energy density

$$(2.3) \qquad U = \sigma\varepsilon + \zeta p,$$

so that the condition $\frac{\partial^2 U}{\partial \zeta \partial \varepsilon} = \frac{\partial^2 U}{\partial \varepsilon \partial \zeta}$, implies $a_{12} = a_{21}$. Letting $a_{11} = 1/K$, where K is the bulk modulus of the elastic phase, $a_{12} = a_{21} = \alpha/K$, with α the Biot–Willis parameter, and $a_{22} = \alpha/(\beta K)$, with β Skempton's coefficient, gives on rearranging (2.1) and (2.2),

$$(2.4) \qquad \sigma = K\varepsilon - \alpha p,$$

$$(2.5) \qquad \zeta = \alpha\varepsilon + \frac{\alpha(1 - \alpha\beta)}{\beta K}p.$$

The system is completed by assuming that the strain is a result of a displacement u and that fluid flow through the porous matrix obeys a Darcy flow model so that the balance of momentum and the conservation of fluid give, if u is the matrix displacement (and neglecting acceleration of fluid through the matrix),

$$(2.6) \qquad \rho\frac{\partial^2 u}{\partial t^2} = \nabla \cdot \sigma,$$

$$(2.7) \qquad \frac{\partial \zeta}{\partial t} = \nabla \cdot \frac{k}{\mu}\nabla p,$$

where ρ is the density of the solid-fluid continuum, k is a permeability, and μ the fluid viscosity. In the model of the brain used in [9], [10], [13], the solid matrix represented the brain parenchyma and the fluid the CSF. In these models, the time scale was long enough that the left hand side of both these equations was neglected, and the time dependence only entered the model in a quasi-stationary manner through a boundary condition that expressed conservation of CSF.

2.2. Two-fluid compartment model for the brain. The simple poroelastic model in (2.6), (2.7) cannot account for changes in blood pressure. Thus [15] postulated, in an appendix to that paper, an extension of the basic Biot theory outlined above to allow multiple, but separate fluid compartments. Here we consider the particular case of a two-fluid model, having a CSF compartment and a blood compartment, both within an elastic structure, and look particularly at the various parameters that arise in this model.

In this case, two more variables have to be introduced, a blood pressure p_b and an increment in blood volume, ζ_b. As before, by linearising the relation between the physical state variables, we obtain

$$\varepsilon = a_{11}\sigma + a_{12}p + a_{13}p_b, \tag{2.8}$$

$$\zeta = a_{21}\sigma + a_{22}p + a_{23}p_b, \tag{2.9}$$

$$\zeta_b = a_{31}\sigma + a_{32}p + a_{33}p_b, \tag{2.10}$$

and we assume the existence of an energy density (see [15] for a more rigorous derivation)

$$U = \varepsilon\sigma + \zeta p + \zeta_b p_b. \tag{2.11}$$

As for a single fluid compartment poroelastic model, the equivalence of mixed derivatives means that the coefficient matrix is symmetric, and $a_{12} = a_{21}$, $a_{13} = a_{31}$ and $a_{23} = a_{32}$. Following the notation above, we rewrite the coefficients of the first equation,

$$a_{11} = \frac{1}{K}, \quad a_{12} = \frac{\alpha}{K}, \quad a_{13} = \frac{\alpha_b}{K}, \tag{2.12}$$

where a subscript b refers to the blood phase. On rearrangement and introducing $\gamma := a_{22} - a_{12}$, $\gamma_b := a_{33} - a_{13}$, $\tilde{\gamma} := a_{13} - a_{23}$,

$$\sigma = K\varepsilon - \alpha p - \alpha_b p_b, \tag{2.13}$$

$$\zeta = \alpha\varepsilon + \gamma p - \tilde{\gamma}p_b, \tag{2.14}$$

$$\zeta_b = \alpha_b\varepsilon - \tilde{\gamma}p + \gamma_b p_b. \tag{2.15}$$

In these equations the coefficients relating stress and strain are the elastic coefficients of the solid matrix, for which there are measurements ([7]). However, the choice of the other coefficients is less certain: leaving the pressures constant, α and α_b describe the rates $\frac{\partial\zeta}{\partial\varepsilon}$ and $\frac{\partial\zeta_b}{\partial\varepsilon}$ at which the CSF and blood volume change when dilating a small element of the porous matrix. If we assume the matrix material, the parenchymal cells, to be incompressible the total volume change has to be accounted for by the sum of the two fluid volumes, that is

$$\alpha + \alpha_b = 1. \tag{2.16}$$

Next, consider the communication of pressure changes between blood and CSF. The blood vessels are viewed as distensible and collapsible tubes, having a different pressure inside than outside, here p_b being the inside and p the outside pressure. This pressure difference is counteracted by the vessel wall, which slightly distends or collapses until it balances the pressure difference. This distension or collapse is of course accompanied by a corresponding change of blood volume inside the vessel, and this blood volume change directly translates into a change of ζ_b. There are models (called tube laws) and measurements of the relation between blood volume ζ_b and transmural pressure difference $p_b - p$. Typically, these tube laws are given in terms of the transmural pressure, $(p_b - p)$ and the ratio of vessel cross-section (or equivalently, the vessel volume) so that this translates into a relation between ζ_b

and $(p_b - p)$. In particular, the blood volume just depends on the pressure difference and not on the single pressures themselves so that we obtain from (2.15) that

$$(2.17) \qquad \tilde{\gamma} = \gamma_b,$$

and at a constant dilation, $\zeta_b = \gamma_b \cdot (p_b - p)$ represents the linearisation of the above-mentioned tube law.

Furthermore, the blood vessels are rather loosely attached to the parenchyma, compared with the tight structure of the neural network. Hence, we expect a dilation of the parenchyma to have rather little effect on the volume of the vessels running through it so that α_b may be assumed very small. As a simplifying model assumption and in absence of real physiological data, we may even assume

$$(2.18) \qquad \alpha_b \approx 0 \quad \text{and thus} \quad \alpha \approx 1.$$

Finally, we shall also propose a model for γ: If, for constant dilation ε, the ICP rises, then the CSF content ζ inside the parenchyma will slightly increase by $\gamma_b(p - p_b)$ due to a small amount of arterial blood being squeezed out of the vessels. A much stronger change of CSF volume is caused by the increased CSF pressure p compressing venous blood vessels inside the brain and thereby reducing overall blood volume, with this volume change being compensated by an increase in CSF volume. Tube laws for blood vessels can again be utilised to describe this mechanism [14] where the volume change of venous blood (and corresponding CSF volume change) is modelled as a function of the transmural pressure difference between CSF and blood, giving a compliance γ_c. Linearisation then allows us to write

$$(2.19) \qquad \zeta = \alpha\varepsilon + \gamma_c p - \gamma_b(p_b - p),$$

so that the overall cerabral compliance is

$$(2.20) \qquad \gamma = \gamma_c + \gamma_b.$$

To summarise, we obtain the state equations

$$(2.21) \qquad \sigma = K\varepsilon - \alpha p - \alpha_b p_b,$$

$$(2.22) \qquad \zeta = \alpha\varepsilon + \gamma p - \gamma_b p_b,$$

$$(2.23) \qquad \zeta_b = \alpha_b \varepsilon + \gamma_b(p_b - p),$$

with $\alpha \approx 1$, $\alpha_b \approx 0$, $\gamma_b = \frac{\partial \zeta_b}{\partial(p_b - p)}$ the (non-dimensional) blood vesssel compliance, and γ the (non-dimensional) parenchymal compliance.

2.3. Poroelastic equations of the brain. The more rigorous derivation in [15] shows that using the actual strain and stress tensors, $\boldsymbol{\varepsilon}$ and $\boldsymbol{\sigma}$, instead of the above-used scalar representations of volumetric strain and stress, (2.21) becomes

$$(2.24) \qquad \boldsymbol{\sigma} = \mathbf{K}\boldsymbol{\varepsilon} - \alpha p \boldsymbol{\delta} - \alpha_b p_b \boldsymbol{\delta},$$

where $\mathbf{K}$ is the stiffness tensor from linear elasticity and $\boldsymbol{\delta}$ the Kronecker tensor, that is, $\boldsymbol{\delta}_{ij} = 1$ for $i = j$ and $\boldsymbol{\delta}_{ij} = 0$ else. Furthermore, in developing a model that incorporates fluctuations on the scale of a heart beat, simple order of magnitude analysis shows that the left-hand side of (2.6) still remains negligible (that is, elastic waves can be ignored) but the time derivative on the left of (2.7) has to be accounted for. Therefore, inserting the poroelastic state equations, we arrive at

$$(2.25) \qquad \nabla \cdot [\mathbf{K}\boldsymbol{\varepsilon} - \alpha p \boldsymbol{\delta} - \alpha_b p_b \boldsymbol{\delta}] = \nabla \cdot [\mathbf{K}\boldsymbol{\varepsilon}] - \nabla \alpha p - \nabla \alpha_b p_b = 0,$$

$$(2.26) \qquad \frac{\partial \zeta}{\partial t} = \frac{\partial \alpha\varepsilon}{\partial t} + \frac{\partial \gamma p}{\partial t} - \frac{\partial \gamma_b p_b}{\partial t} = \nabla \cdot \frac{k}{\mu} \nabla p.$$

As described in the previous section, all parameters are just linearisations of the stresses $\boldsymbol{\sigma}$ and fluid contents ζ and ζ_b with respect to the strains $\boldsymbol{\varepsilon}$ and the pressures p and p_b. Since these linearisations are performed around a specific state of $\boldsymbol{\sigma}, \zeta, \zeta_b, \boldsymbol{\varepsilon}, p, p_b$, they will in general change as p, p_b, and $\boldsymbol{\varepsilon}$ change. However, γ_b may roughly be approximated as constant ([15]), and $\alpha \approx 1$ as well as $\alpha_b \approx 0$ will also stay a valid approximation, whereas γ_c is expected to vary with ICP. We make a further modelling assumption, that the parameter γ_c changes slowly and is a function of the average pressure, and not the instantaneous pressure. Denoting $\bar{p}$ as ICP averaged over some period of several heartbeats,

$$(2.27) \qquad \bar{p}(x,t) = \frac{1}{T} \int_{t-T}^{t} p(x,t)\mathrm{d}t,$$

where $T = 2 - 3$ seconds and assuming that $\bar{p}$ is varing very slowly with time, the derivatives on the left of (2.26) can be simplified and we solve

$$(2.28) \qquad \nabla \cdot [\mathbf{K}\boldsymbol{\varepsilon}] - \alpha\nabla p - \alpha_b \nabla p_b = 0,$$

$$(2.29) \qquad \alpha\frac{\partial\varepsilon}{\partial t} + \gamma(\bar{p})\frac{\partial p}{\partial t} - \gamma_b\frac{\partial p_b}{\partial t} = \nabla \cdot \frac{k}{\mu}\nabla p.$$

In [14] a non-dimensional venous compliance, γ_c, was determined by

$$(2.30) \qquad V_{\mathrm{parenchyma}}\gamma_c(p) = \frac{1}{E(p - p_r)^n}$$

where E, n and p_r are constants that were related to the mechanical structure of compressed veins and $V_{\mathrm{parenchyma}}$ is the parenchyma volume. Integrating this relation over the parenchyma, ignoring spatial variation of pressure yields the overall cerebral compliance,

$$(2.31) \qquad C(p) = \frac{\partial V_{\mathrm{CSF}}}{\partial p} = V_{\mathrm{parenchyma}}\gamma(p) = V_{\mathrm{parenchyma}}\gamma_b + \frac{1}{E(p - p_r)^n}.$$

In this we can identify an arterial compliance by $C_b = V_{\mathrm{parenchyma}}\gamma_b$ but since the dimensionless arterial compliance γ_b is much smaller than the venous counterpart, $\gamma_c(p)$, and letting $n = 1$, (2.31) reduces to the compliance law in [6].

We will approximate the parenchyma as a spherical shell with outer radius c and inner radius a, in which the system (2.28) and (2.29) has to be solved. Furthermore, we assume a constant CSF production Q_p inside the brain ventricles (at $r = a$) and a (time-dependent) liquid infusion at rate Q_i at $r = c$. Finally, there will be CSF absorption at $r = c$ at a rate $\frac{p - p_{ss}}{\mu R}$, where p_{ss} is the sagittal sinus pressure and R a resistance, and the ventricles are connected to the outer boundary of the brain by a single thin canal of length $L = c - a$, the aqueduct, through which we have Poiseuille flow. We denote the radial displacement of the parenchyma by u and assume the solid matrix stress to be given by Hooke's law with Lamé constants λ and G, that is, $\mathbf{K}\boldsymbol{\varepsilon} = \lambda(\mathrm{tr}\boldsymbol{\varepsilon})\boldsymbol{\delta} + 2G\boldsymbol{\varepsilon}$. Using spherical symmetry, the governing equations are

$$(2.32) \qquad (\lambda + 2G)\left(\frac{\partial^2 u}{\partial r^2} + \frac{2}{r}\frac{\partial u}{\partial r} - \frac{2u}{r^2}\right) - \alpha\frac{\partial p}{\partial r} - \alpha_b\frac{\partial p_b}{\partial r} = 0,$$

$$(2.33) \qquad \alpha\frac{\partial}{\partial t}\left(\frac{\partial u}{\partial r} + \frac{2u}{r}\right) + \gamma(\bar{p})\frac{\partial p}{\partial t} = \frac{1}{r^2}\frac{\partial}{\partial r}\left(\frac{k}{\mu}r^2\frac{\partial p}{\partial r}\right) + \gamma_b\frac{\partial p_b}{\partial t}.$$

Furthermore, the PDEs will be complemented by one boundary condition for the pressure and for the displacement at each boundary. In particular, we will use CSF conservation in the subarachnoid space,

$$(2.34) \qquad \frac{p - p_{ss}}{\mu R} = \frac{\pi d^4}{128 \mu L}(p|_{r=a} - p) - 4\pi c^2 \frac{k}{\mu} \frac{\partial p}{\partial r} + Q_i \ \text{ at } r = c,$$

zero displacement at the skull,

$$(2.35) \qquad\qquad\qquad\qquad u = 0 \ \text{ at } r = c,$$

flux conservation in the ventricles,

$$(2.36) \qquad 4\pi a^2 \frac{\partial u}{\partial t} = -\frac{\pi d^4}{128 \mu L}(p - p|_{r=c}) + 4\pi a^2 \frac{k}{\mu} \frac{\partial p}{\partial r} + Q_p \ \text{ at } r = a,$$

and continuity of stresses at the ventricle walls,

$$(2.37) \qquad\qquad (\alpha - 1)p = (\lambda + 2G)\frac{\partial u}{\partial r} + 2\lambda \frac{u}{r} - \alpha_b p_b \ \text{ at } r = a.$$

The system of equations, (2.32)-(2.37), once values are assigned to constants, can be solved using as input only the arterial pressure, $p_b(t)$ and the infusion rate, $Q_i(t)$. We have calculated solutions using both finite difference and finite element discretisations. The solutions below are from using a central difference in space and simple implicit Euler integration in time. The solutions show that the pressure is almost constant spatially.

2.4. Neglecting blood pressure fluctuations. Setting $\gamma_b = 0$ removes any dependence on blood pressure fluctuations. Solution for ICP for the parameter values $\mu R = 15$ mmHg sec/ml and $E = 0.24$ ml^{-1} is shown in figure 1 where the computed ICP is shown with an average observed ICP (the average being a running average over a 2 second window, see (2.27)). This provides a very reasonable prediction of mean ICP. In figure 2 the spatial and temporal variation is illustrated for this calculation. Results are shown for displacement, strain, pressure and water increment. The ventricle displacement is very small throughout the simulation and with such small strain, the use of linear elasticity should be satisfactory for such simulation. During the test the ventricle slightly dilates and there is a very small displacement through the parenchyma. There is a corresponding increase in CSF content very near the ventricles as the underlying matrix is stretched sideways but further out, compression leads to a slight decrease in CSF content.

2.5. Influence of blood pressure fluctuations. When the blood pressure parameter, γ_b, is not zero then blood pressure oscillations are included in calculations. A typical computation using an implicit time stepping method is shown in figure 3 where the parenchyma displacement, strain, ICP and change in CSF content are very similar to those shown in figure 1 in the absence of arterial pressure fluctuations. Values for strain and change in water content are very close because of the definition (2.14). While the values calculated near the ventricles are a little higher during the test, the displacement, strain and change in water content are not significantly different whether blood pressure fluctuations are accounted for or not. The calculated ICP is, however, considerably different from that when γ_b is zero. This is shown in figure 4 where the calculated and observed ICP are shown together with a running mean for ICP and the amplitude of oscillation. The mean ICP is calculated using (2.27) and the amplitude of oscillation by

$$(2.38) \qquad\qquad \text{Amplitude}(t) = \left[\frac{1}{T} \int_{t-T}^{t} (p - \bar{p})^2 \mathrm{d}t \right]^{0.5}.$$
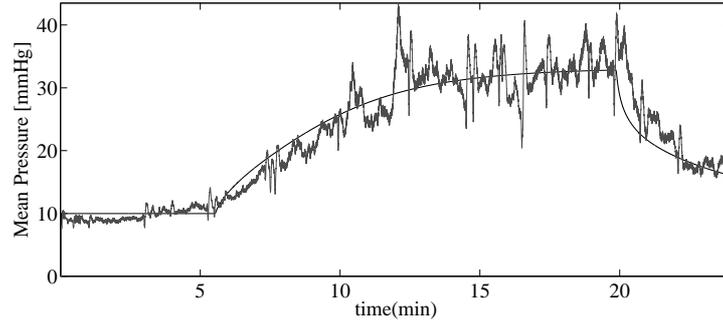
FIGURE 1. Comparison of predicted ICP against observed ICP in an infusion test without accounting for blood pressure oscillations. The solid line is computed ICP, measured ICP is shown in grey. The infusion injected $Q_i = 1.5$ ml/min between $t = 5.5$ and $t = 19.9$ mins.
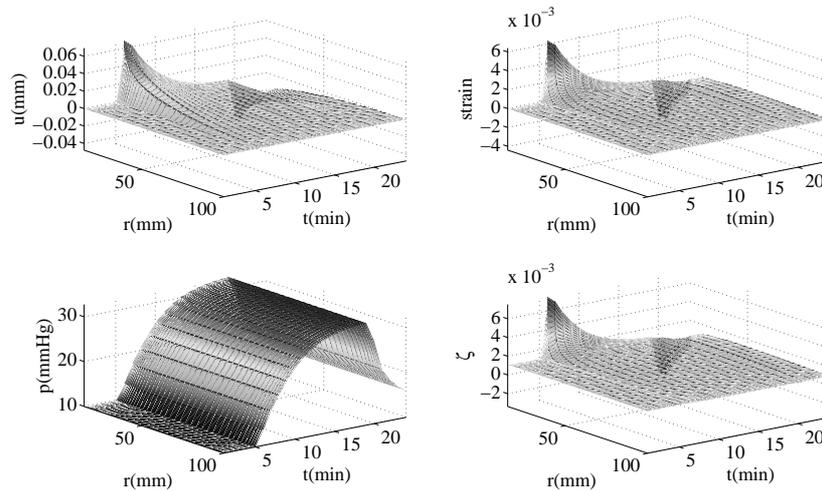

FIGURE 2. Spatial and temporal variation during infusion test without accounting for blood pressure oscillations; (a) Radial displacement, (b) strain, (c) ICP, (d) change in CSF content.

There are periodic spikes caused by periodic interruption of the observed clinical data by another device. Both the mean ICP and amplitude of oscillation are predicted well by the model but it is also clear from the un-averaged ICP that there are slow periodic events in the clinical data that are not predicted by the model. If we look at the ICP response in detail, see figure 5, then some limitations of the model are apparent. The mean value is clearly very well predicted as is the amplitude of ICP oscillations but there are unexplained phase differences, particularly in the time of peak ICP.
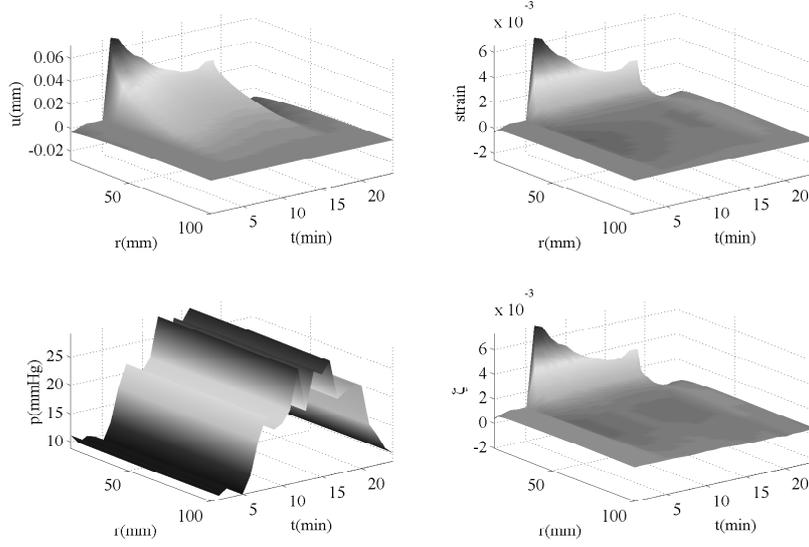
FIGURE 3. Spatial and temporal variation during infusion test including blood pressure oscillations; (a) Radial displacement, (b) strain, (c) ICP, (d) change in CSF content. Data every minute was used to generate graphs.

3. Space averaged model

The governing equations for the spatially varying model are time consuming to solve numerically and such calculated solutions show that the CSF pressure is almost constant through the parenchyma, with very thin layers near the ventricles and near the skull. Given this lack of spatial dependence in the solutions, it is worth examining the space integral form of those equations under an assumption of spatially constant pressure (that is that ICP is a funtion only of time).

Taking a space integral of various terms and using $\varepsilon = \dfrac{1}{r^2}\dfrac{\partial r^2 u}{\partial r}$, one obtains

$$(3.1) \qquad \int_a^c 4\pi r^2 \varepsilon \, \mathrm{d}r = -4\pi a^2 u(a),$$

using $u(c) = 0$, and

$$(3.2) \qquad \int_a^c 4\pi r^2 \gamma(\bar{p})\frac{\partial p}{\partial t}\mathrm{d}r \approx V_{\text{parenchyma}}\gamma(\hat{p})\frac{\mathrm{d}\hat{p}}{\mathrm{d}t},$$

where $\hat{p} = \hat{p}(t)$ is now the spatially constant pressure. Applying this to (2.33) we obtain

$$(3.3) \qquad -4\pi a^2 \alpha \frac{\mathrm{d}u(a,t)}{\mathrm{d}t} + V_{\text{parenchyma}}\left[+\gamma(\hat{p})\frac{\mathrm{d}\hat{p}}{\mathrm{d}t} - \gamma_b\frac{\mathrm{d}p_b}{\mathrm{d}t}\right] = 4\pi\frac{k}{\mu}r^2\frac{\partial p}{\partial r}\bigg|_a^c.$$

However, adding the boundary conditions (2.34) and (2.36)

$$(3.4) \qquad 4\pi\frac{k}{\mu}r^2\frac{\partial p}{\partial r}\bigg|_a^c = Q_p + Q_i - 4\pi a^2\frac{\mathrm{d}u(a,t)}{\mathrm{d}t} - \frac{p(c,t) - p_{ss}}{\mu R},$$
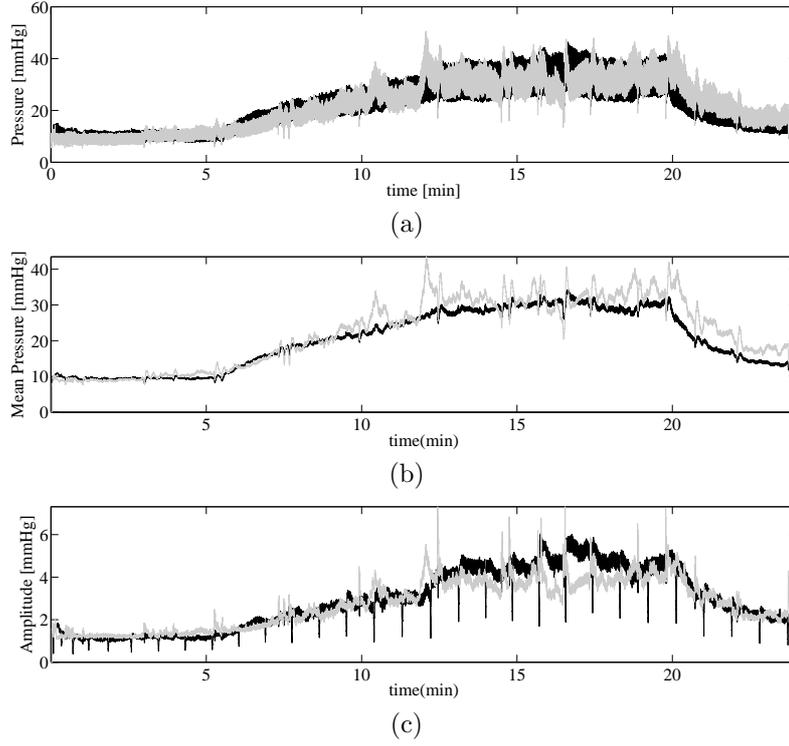
FIGURE 4. Computed ICP variation during infusion test including blood pressure oscillations. In each figure the computed data is in black and clinical data in grey. (a) ICP versus time during the test. (b) Time averaged ICP, (c) Time averaged amplitude of oscillation.
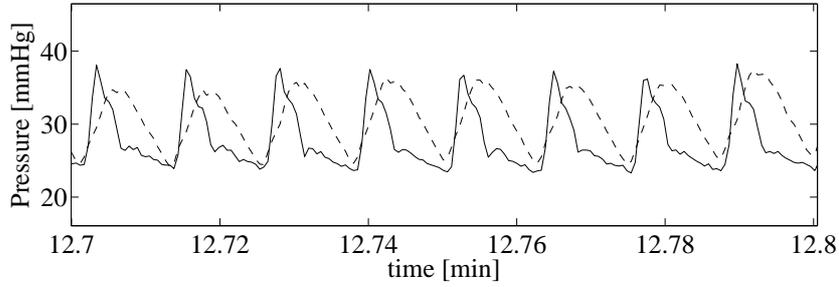

FIGURE 5. ICP variation during a small part of infusion test: (——) Calculated values, (- - -) clinical data.

defining a base ICP, p_1, by

$$(3.5) \qquad Q_p = \frac{p_1 - p_{ss}}{\mu R},$$

and assuming that blood pressure is also spatially constant,

$$(3.6) \qquad C(\hat{p})\frac{\mathrm{d}\hat{p}}{\mathrm{d}t} + \frac{\hat{p} - p_1}{\mu R} = Q_i + 4\pi a^2(\alpha - 1)\frac{\mathrm{d}u}{\mathrm{d}t}(a, t) + C_b\frac{\mathrm{d}p_b}{\mathrm{d}t}.$$

This is a very interesting result: excepting the second and third terms on the right, it is the one compartment model that has been widely used [6],

$$(3.7) \qquad C(\hat{p})\frac{\mathrm{d}\hat{p}}{\mathrm{d}t} + \frac{\hat{p} - p_1}{\mu R} = Q_i.$$

Of course if $\alpha < 1$ then the ventricle displacement is undetermined and this equation cannot be solved but in the case we are considering, when $\alpha = 1$, the equation is independent of the underlying poro-elastic framework, becoming a non-linear ODE

$$(3.8) \qquad C(\hat{p})\frac{\mathrm{d}\hat{p}}{\mathrm{d}t} + \frac{\hat{p} - p_1}{\mu R} = Q_i + C_b\frac{\mathrm{d}p_b}{\mathrm{d}t}.$$

This is a significant simplification since integration of an ODE is less computationally difficult than solving time dependent PDEs yet the effect of blood pressure oscillations on ICP fluctuations remains inherent in this model. There are some existing models that incorporate blood pressure oscillations, for example, [1] develop an electrical analogue model that allows CSF pulsations, see also [5].

In order to examine the effect of pulsatility, define two time scales,

$$(3.9) \qquad \tau = \mu R, \quad \tau_b = \mu R C_b,$$

and a pressure, p_2,

$$(3.10) \qquad p_2 = p_1 + \mu R Q_i.$$

The pressure p_2 is the plateau in average pressure that should be achieved in the infusion test.

Using this notation, the reduced equation is

$$(3.11) \qquad \tau\frac{\mathrm{d}\hat{p}}{\mathrm{d}t} + \hat{p} = p_2 + \tau_b\frac{\mathrm{d}p_b}{\mathrm{d}t}.$$

For the infusion test we have shown results above, $\tau \sim 750$ sec, $\tau_b \sim 60$ sec, $p_1 \sim 10$ mmHg, $p_2 \sim 33$ mmHg and $|\frac{\mathrm{d}p_b}{\mathrm{d}t}| \sim 240$ mmHg/s.

The reduced equation (3.11) is, if τ is approximately constant, just a linear ODE and so in that case, can be solved using a Laplace transform. In particular if we suppose $\hat{p}(0) = p_1$, and

$$(3.12) \qquad p_b(t) = P_b + \sum_{k=1}^{\infty} a_k \cos(\omega_k t),$$

where P_b is the mean blood pressure, a_k are Fourier components and ω_k are associated frequencies, then the solution for $\hat{p}$ is

$$(3.13) \quad \hat{p}(t) = p_1 \mathrm{e}^{-t/\tau} + p_2(1 - \mathrm{e}^{-t/\tau}) + \sum_k^{\infty} \frac{\tau_b \tau a_k \omega_k^2}{1 + \omega_k^2 \tau^2}[\cos \omega_k t - \mathrm{e}^{-t/\tau} - \frac{1}{\omega_k \tau}\sin \omega_k t],$$

and the pressure will fluctuate about p_2 at large times.

The nonlinear equation is more difficult to analyse but a simpler version, obtained when we set $p_r = 0$ in (2.31), or equivalently, redefine the dependent variable to be the offset $\hat{p} - p_r$, has $\tau(p) \sim 1/p$. Letting $\tau_0 = \tau(p_1)$, and considering just one Fourier component of natural frequency Ω, (with $\Omega \sim 1.8$Hz in the test above and $\omega_1 = 2\pi\Omega$) then (3.11) becomes

$$(3.14) \qquad \frac{\tau_0 p_1}{\hat{p}}\frac{\mathrm{d}\hat{p}}{\mathrm{d}t} + \hat{p} = p_2 - 2\pi\tau_b\Omega a_1 \sin 2\pi\Omega t, \quad \hat{p}(0) = p_1,$$

where the constant $2\pi\tau_b\Omega a_1$ incorporates the blood compliance time scale and the amplitude of blood pressure oscillation.

This nonlinear equation does have an analytic solution,

$$(3.15) \qquad \hat{p}(t) = \frac{p_1 e^{[\frac{p_2 t}{p_1 \tau_0} + \frac{\tau_b a_1}{\tau_0 p_1} \cos 2\pi\Omega t]}}{\frac{1}{\tau_0} \int_0^t e^{[\frac{p_2 s}{p_1 \tau_0} + \frac{\tau_b a_1}{\tau_0 p_1} \cos 2\pi\Omega s]} ds + e^{\frac{\tau_b a_1}{p_1 \tau_0}}}$$

This analytic form is difficult to use because of the increasing exponentials in both numerator and denominator, it is possible to divide out the exponentials from both numerator and denominator but the resulting integral in the denominator remains problematic to evaluate accurately. Time marching integration of the nonlinear differential equation requires considerable care, we have used a fourth order Runge Kutta as well as built in MATLAB routine `ode23s` successfully, lower order methods (Euler or second order Runge-Kutta) have failed and using them for simulations is likely to lead to misleading interpretation of parameter values.

To illustrate application of the space averaged model to an infusion test, we show in figure 6 the result of a computation of ICP using a fourth order Runge-Kutta integrator without averaging of ICP for the compliance and the same parameter values as used to compute the result shown in figure 1. As with the spatially varying model, slow changes in mean ICP are not calculated but the mean ICP and amplitude of ICP oscillations is predicted reasonably well.

4. Summary

We have developed models for the CSF infusion test which incorporate arterial pressure pulsations and applied the models to data from an infusion test. Results using a spherically symmetric model give some insight into how the parenchyma is affected during an infusion test but these have to be considered in the light of the very simple geometry used. The computations show that the average ICP and amplitude of ICP oscillations can be modelled well, although the detailed shape of the observed ICP curve with time is not fully matched, indicating that there are important effects which are not yet in the model. There are slow changes in the ICP during the test which are also not predicted: the source of such slow waves may be a result of autonomous changes within the brain during the test and so not predictable in anycase by what is only a mechanical model.

When the spatial dependence is removed from the multi-compartment poroelastic model, a simple ODE emerges but with properties that need more study and understanding if the model is to be used to infer parameter values. We have considered the very simplest model that included blood pressure oscillations, an extension will be to consider two blood compartments, arterial and venous, assuming that arterial pressure fluctuations are those given from measurements and that venous pressure is approximately constant.

References

[1] M Bergsneider, A.A. Alwan, L. Falkson, and E.H. Rubinstein. The relationship of pulsatile cerebrospinal fluid flow to cerebral blood flow in tracranial pressure: a new theoretical model. *Acta Neurochirurgica Supplementum*, 71:266–268, 1998.

[2] M. Biot. General theory of three dimensional consolidation. *Journal of Applied Physics*, 12:55–164, 1941.

[3] M. CZosnyka, Z. Czosnyka, S. Momjian, and J. Pickard. Cerebrospinal fluid dynamics. *Physiological Measurement*, 25:R51–R76, 2004.
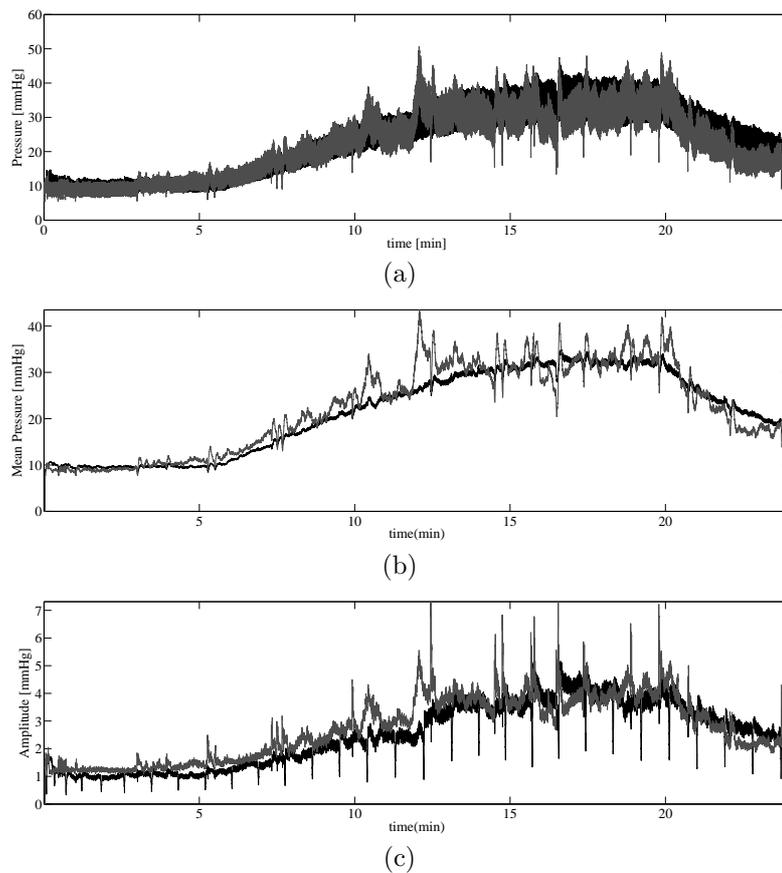
(a)

(b)

(c)

FIGURE 6. Computed ICP variation during infusion test including blood pressure oscillations using the space averaged model. In each figure the computed data is in black and clinical data in grey. (a) ICP versus time during the test. (b) Time averaged ICP, (c) Time averaged amplitude of oscillation. Parameter values are the same as used in figure 1.

[4] M. Czosnyka and J. D. Pickard. Monitoring and interpretation of intracranial pressure. *J Neurol Neurosurg Psychiatry*, 75:813–821, 2004.

[5] M. Egnor, A. Rosiello, and L. Zheng. A model of intracranial pulsations. *Pediatr Neurosurg*, 35:284–298, 2001.

[6] H. Juniewicz, M. Kasprowicz, M. Czosnyka, Z. Czosnyka, S. Gizewski, M. Dzik, and J. D. Pickard. Analysis of intracranial pressure during and after the infusion test in patients with communicating hydrocephalus. *Physiological Measurement*, 26:1039–1048, 2005.

[7] K. Miller. Constitutive model of brain tissue for finite element analysis of surgical procedures. *Journal of Biomechanics*, 32:475–479, 1999.

[8] S. Sivaloganathan, J. Drake, and G. Tenti. Mathematical pressure volume models of the cerebrospinal fluid. *Applied Mathematics and Computation*, 94:243–266, 1998.

[9] A. Smillie, I. Sobey, and Z. Molnar. A hydroelastic model of hydrocephalus. *Journal of Fluid Mechanics*, 539:417–443, 2005.

[10] I. Sobey and B. Wirth. Effect of non-linear permeability in a spherically symmetric model of hydrocephalus. *Mathematical Medicine and Biology*, 23:339–361, 2006.

[11] H. Wang. *Theory of Linear Poroelasticity: with Applications to Geomechanics and Hyrdo-geology.* Princeton University Press, 2002.

[12] R. A. Weerakkody, M. Czosnyka, M. U. Schuhmann, E. Schmidt, N. Keong, T. Santarius, J. D. Pickard, and Z. Czosnyka. Clinical assessment of cerebrospinal fluid dynamics in hydrocephalus. guide to interpretation based on observational study. *Acta Neurologica Scandinavica*, 2011.

[13] B. Wirth and I. Sobey. An axisymmetric and fully 3d poroelastic model for the evolution of hydrocephalus. *Mathematical Medicine and Biology*, 23:363–388, 2006.

[14] B Wirth and I. Sobey. A model for an inverse power constitutive law for cerebral compliance. *Mathematical Medicine and Biology*, 25:113–131, 2008.

[15] B Wirth and I. Sobey. Analytic solution during an infusion test of the linear unsteady poroelastic equations in a spherically symmetric model of the brain. *Mathematical Medicine and Biology*, 26:25–61, 2009.

Mathematical Institute, University of Oxford, Oxford, England
E-mail: `ian.sobey@maths.ox.ac.uk and eisentraeger@maths.ox.ac.uk`

Institute for Numerical Simulation, University of Bonn, Endenicher Allee 60, 53115 Bonn, Germany
E-mail: `benedikt.wirth@ins.uni-bonn.de`

Academic Neurosurgical Unit, Addenbrookes Hospital, Cambridge, England
E-mail: `mc141@medschl.cam.ac.uk`